Towards a Pre-diagnose of Surgical Wounds through the Analysis of Visual 3D Reconstructions

Neus Muntaner Estarellas[3], Francisco Bonin-Font[1], Juan J. Segura-Sampedro[2],
Andres Jiménez Ramírez[3], Pep L. Negre Carrasco[1], Miquel Massot Campos[1],
Francesc X. Gonzalez-Argenté[2] and Gabriel Oliver Codina[1]

[1]*Department of Mathematics and Computer Engineering, University of the Balearic Islands,*
Ctra. Valldemossa Km 7.5, 07122 Palma de Mallorca, Spain
[2]*Department of General and Digestive Surgery, University Hospital Son Espases,*
07122 Palma de Mallorca, Spain
[3]*Group of Ingeniería Web y Testing Temprano, Department of Languages and Computing Systems, University of Sevilla,*
c/ San Fernando 4, 41004 Sevilla, Spain

Keywords: 3D Visual Reconstruction, Structure From Motion, Post-surgical Wound, Telemedicine.

Abstract: This paper presents a new methodology to pre-diagnose the state of post-surgical abdominal wounds based on visual information. The process consist of four major phases: a) building dense 3D reconstruction of the abdominal area around the wound, b) selecting an area close to the wound to fit a plane, c) calculating the distance from each point of the 3D model to the plane, d) analyzing this map of distances to infer if the wound is inflamed or not. This method needs to be wrapped in an application to be used by patients in order to save unnecessary visits to the medical center.

1 INTRODUCTION

The emergency and the outpatient facilities of the Spanish public health care system are usually collapsed by the numerous of unnecessary visits to the assistance centers that could be solved at home with several indications given by the corresponding specialist.

In 2017, more than 3000 operations were done in the University Hospital Son Espases, in Palma de Mallorca, from which, only approximately the half of them were programmed. That makes a mean of 250 patients per month, 63 patients per week, and 13 patients per day. If the consult mean time in Spain is intended to range between 6 and 10 minutes, it makes a mean of 2 hours a day dedicated only to take care of post surgery wounds, without taking into consideration the rests of tasks, such as, new patients, non surgery patients, management meetings or emergencies.

Every surgery patient is evaluated twice after the surgical procedure. The first review is at the health center after a week. And it is evaluated again one month later as outpatient, at the hospital. One of the main reasons for this evaluation is to check the surgical wound and detect its infection. However the rate of infection is low and when it happens it is usually detected in the emergency department.

This face-to-face consultations, where most of them present no anomalies, could be easily managed remotely, having a cheaper cost and affecting less the patients' quality of life, as they require unnecessary transfers to the health facility and absences from work. Moreover, if the patient is unable to suspect the wound infection on time, as it usually happens, an increase of the emergency department consultations is produced, normally with a delay in the wound infection diagnosis which results in an increase of visit time per patient.

Consequently, every technological progress in the field of health care management, in general, and in the post-surgery assistance in particular, is very useful to reduce the costs, to improve the quality of assistance time and thus to increase the quality of life of the patients. Medical computer and mobile applications focused on remote automatic diagnose and patient management/monitoring have been advancing in the last years citenephroflow, (Topdoctors, 2017). Lately, some studies in telemedicine support the feasibility and safety of remote follow-up in surgical wounds

and the patients satisfaction (Segura-Sampedro et al., 2017). In this later reference as well as in similar studies (Nordheim et al., 2014), photos or videos of the wound and filled questionnaires constitute the exchanged data between the patient and the doctor, but is the doctor who always analyzes and evaluates the received information. However, to our knowledge, none of the revised methods or Apps is able to estimate, automatically, a reliable pre-diagnose based on visual data, and to filter out those wounds that clearly present a good evolution, without the intervention of the physician. Following this line, the Department of General and Digestive Surgery of the University Hospital Son Espases is collaborating with the Systems, Robotics and Vision group of the University of the Balearic Islands, in order to go one step forward in the design and implementation of a vision-based mobile App for telemedicine that can help in the estimation of a pre-diagnose of abdominal post surgery wounds. The objective is filtering, automatically, those wounds that potentially present inflammation as sign of infection and need a face-to-face evaluation in the hospital from those that course a normal evolution and can be managed at home, saving time and medical resources. The novelty of this work is more in the methodology itself and the application than in the pipeline of visual algorithms designed to get the objective. This method needs to be wrapped into a future compact mobile App, which will contain additional functionalities to increase the communication and data exchange between doctors and patients.

The wound analysis process consists of a pipeline that involves the next steps: a) grab a video sequence, with the mobile, of the abdominal zone around the wound, from side to side, viewing the same area but from different perspectives and viewpoints, b) extract images of the video sequence, c) extract and track common visual features in all the images, d) build a 3D sparse point cloud using a *Structure From Motion* (SFM) (Hartley and Zisserman, 2003) algorithm, e) build a dense point-cloud and a textured meshed surface, f) establish a polyline and a plane fitted in this polyline in a selected portion of the 3D model; this plane is intended to be, either tangent to the abdomen surface, or crossing the abdominal area, below the wound, g) compute the distance between each point of the 3D model and the plane, and emit a diagnose function of these distances.

2 METHODOLOGY

Firstly, the patient must record with the mobile telephone a video of the wound, from side to side of the abdominal area, in order to have views from different perspectives and viewpoints. The second step is automatic and consist of extracting all the images from the video sequence. Once the images have been extracted, the process of 3D reconstruction starts automatically with the feature tracking process. The SFM geometric theory (Hartley and Zisserman, 2003) is based on the tracking of a set of world points projected in several images taken by the same camera from different viewpoints. These projected points and their correspondences in the subsequent images are obtained thanks to a process of a classical visual feature detection and matching (Hartley and Zisserman, 2003) using two reputed detectors invariant to rotation and scale: one detector with scalar descriptor, SIFT (Lowe, 2004), and one detector with binary descriptors, ORB (Rublee et al., 2011). Both techniques have proved extendedly his excellent performance in terms of number of features, robustness and traceability. Invariance to scale and rotation is important for this kind of application since the image key points must be identified in all frames of the video sequence, which show the affected area from different viewpoints. Figure 1 shows an image provided by the University Hospital Son Espases of a surgical wound, with the visual features obtained using the 2 different detectors.

| (a) | (b) |

Figure 1: Feature detection with: (a) SIFT, (b) ORB.

The feature detection with the 2 tested features has been implemented with the feature detector OpenCv2 functions. The descriptor matching has been implemented with the FLANN (Muja and Lowe, 2009) matcher library. Good matches (inliers) are considered to be those which distance between correspondences in different images is under a certain threshold (typically, either 0.02 or 2 times the minimum distance between all the matches). Bad matches are discarded.

Given the projection matrices, the 3D coordinates of a world point can be obtained from its corresponding image points (in this case visual features) identified in several views (matching) using triangulation. Ideally, the 3D point should lie in the intersection of all back-projected rays. But, in general, these rays will not intersect in a single point due to the errors inherent to the feature matching process. The 3D coordinates of the world point are obtained minimizing the

sum of squared errors between the measured and the predicted image positions of the 3D point projected in all involved views where the world point is visible: $X = \arg\min_x \sum_i \|u_i - \hat{u}_i\|^2$, where u_i is the predicted image point and $\hat{u}_i$ is the corresponding measured image point, for all the i images where the 3D point is projected. The predicted image point can be obtained, for example, from the feature matching process, and the measured point is directly the projection of the world point on the image.

The library OpenMVG (Moulon et al., 2017) implements the point triangulation and the 3D recovery applying the SFM and the epipolar theories, recovering also the camera displacement, and has been used to form sparse 3D point-clouds from input sets of images. OpenMVS (cDcSeacave, 2017) provided us with a complete set of algorithms to recover a full, fine and textured surface from a set of camera poses and a sparse point-cloud.

Figure 2 illustrates the image processing pipeline designed and implemented to obtain a dense 3D model of the recorded area. The four first steps have been programmed with OpenMVG, and the last four steps with OpenMVS. The SFM implementation is based on (Moulon et al., 2013). This process is incremental, which means that, the first reconstruction is done only with two views, and at every iteration a new view is incorporated adding features, some matching with the previous and needing triangulation, some new in the scene. The reconstruction with known poses refers to the process of refining the 3D model using the camera poses and the 3D point position relative to the know camera poses, once the SFM and the camera motion have been computed. The point cloud densification is based on (Barnes et al., 2009), the mesh reconstruction is based on (Jancosek and Pajdla, 2014), the mesh refinement is based on (Vu et al., 2012), and finally, the mesh texturing is based on (Waechter et al., 2014).
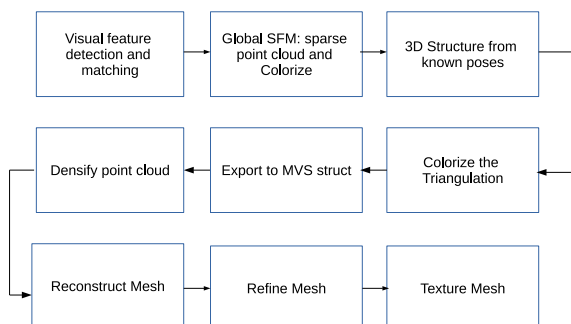
Figure 2: Image processing pipeline for wound 3D reconstruction.

A 3D reconstruction of an abdominal area with a post surgical wound is presented in figure 3 as
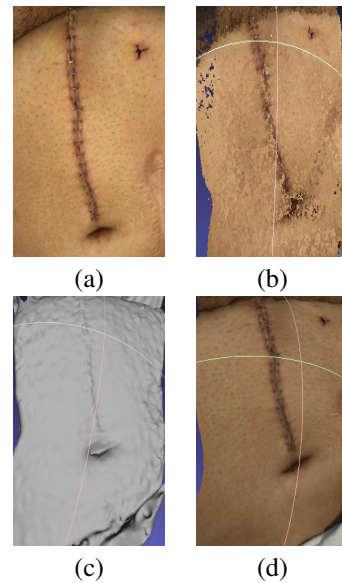
Figure 3: A result of the 3D reconstruction pipeline: (a) a frame of the recorded video, (b) the dense point cloud, (c) refined mesh, (d) refined and textured mesh.

a sample of the pipeline performance. 130 frames were extracted from the video. One sample image is shown in figure 3-(a) and the video can be seen in https://youtu.be/XW18WMFZPTw. The appearance of the reconstructed abdomen is highly realistic, but without a metric scale it is impossible to infer the 3D structure dimensions.
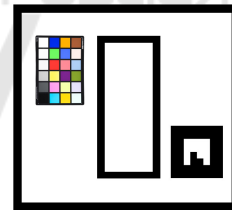
Figure 4: Template used to scale the obtained 3D model.

The obtained 3D model has no metrical units, since it is computed from the images and the visual feature coordinates which are expressed in pixels. Converting these data into metrical data was necessary to estimate the wound state from the 3D reconstruction. To this end, the geometric template of figure 4 was designed. This template contains one color calibration pattern, not yet used in this work, one geometrical marker which side measures $3.1cm$ and a rectangular hole in between. The template must be placed on the abdomen with the wound falling just inside the rectangular hole. Once the template is correctly placed, the video can be recorded. The scale ratio applicable to all reconstructed 3D points can be calculated dividing the marker side real metric

by its length measured in the 3D model. A sample of a video recorded with the template can be seen at https://youtu.be/INtkQlNXbu0.

In order to perform the last steps of the pipeline which include the plane fitting and the distance calculation, the resulting 3D point cloud was opened with Cloud Compare (Girardeau-Montaut, 2017). Using this application, the 3D volume was cropped around the wound and scaled according to the measures provided by the marker of the template (if it was available). Afterwards, a polyline was created inside the processed 3D volume to fit a plane inside it. This plane was intended to be, either coincident with the plane of the marker, or parallel to it, tangent to the abdomen surface, just at the wound base, or cutting the abdomen surface in four points, below the wound. Finally, the distance of each point of the cloud to the fitted plane was calculated and exported to a *csv* file. The analysis of these distances for each case leads to an attempt of estimated diagnose.

3 EXPERIMENTS

In order to evaluate the complete procedure, some simulated experiments were initially performed using the template and a small cable with a diameter of $4mm$ simulating an inflamed wound. Figure 5-(a) shows an image of one simulated scene.

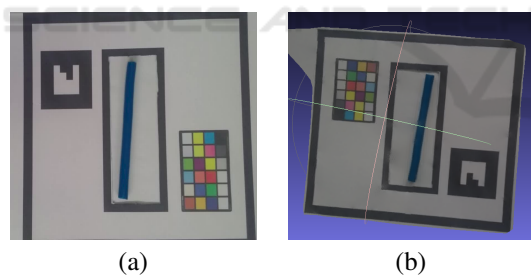(a)   (b)

Figure 5: Simulated wound: (a) an image of the simulated scene, (b) the textured mesh.

The length of the marker side in the 3D reconstruction, measured in Cloud Compare was 0.122898 units. Knowing that the real length of the marker side is 3.1cm, the scale factor set in Cloud Compare for the 3 directions (x, y, z) was $0.031(m)/0.122898 = 0.25224169m$. In this case, the fitted plane was coincident with the plane of the marker. Figure 5-(b) shows the textured mesh.

Figure 6 shows the selected volume in yellow (a), the same volume with the fitted plane (border in white and plane area in blue) in (b), and the spatial map of distances between all points of the selected volume and the fitted plane, in (c). Notice how the pos-

itive (yellow-orange) distances range between $2mm$ and $4mm$, along the rectangle, clearly differentiating the cable profile from the surrounding area (blue). Lying the fitted plane on the template, these positive distances coincide approximately with the cable diameter.

Figure 7-(a) shows an image of another inflamed wound simulated with a small cable. Figures 7-(b), 7-(c) and 7-(d) show, respectively, the refined and textured mesh, the selected volume in yellow with the polyline fitting plane in white and the map of distances from points to the plane. The scale factor resulted in $0.031m/0.0611679 = 0.50680177m$, being 0.0611679 the marker side length measured in Cloud Compare. The map of distances shows clearly the linear shape of the simulated inflamed wound in the center of the rectangle with positive distances around $3mm$ surrounded by points that mark negative distances below $-4mm$.

Figure 8-(a) shows the selected volume in yellow around the wound of figure 3 with the polyline fitting the plane in white. In this case, the plane intersects the abdomen below the wound, in one part, and above, in another. This is a case of a wound with a good evolution, without inflammation. Figure 8-(b) shows the corresponding map of distances to the fitted plane. The central area in yellow indicates where the plane is below the wound and the distance is bigger while the extremes which tend to blue indicate where the distance is smaller. In this case, the metric units and values have no relevance. Since there are no points in the center of the map that mark the shape of the wound, one can conclude that most likely there is no inflammation on the explored area.

Figure 9-(a) shows an image extracted from a video of another example of post surgical wound with a good evolution and no inflammation. In this case the scale is also irrelevant. 35 images were extracted to build the refined and textured 3D model, shown in figure 9-(b). In this experiment, the plane was fitted below the abdomen as shown in white in figure 9-(c). The map of distances is show in figure 9-(d). The later shows clearly the difference between the central area with positive distances corresponding to the zone with maximum curvature of the abdomen (maximum distance to the plane), and both sides (top and bottom) where the distance between the plane and the abdomen is minimum, without any part suggesting the presence of any inflamed area in the form of a transversal line of distances clearly above the rest. These type of resulting plot would suggest to the patient and to the doctor, in principle, an unnecessary face-to-face revision.
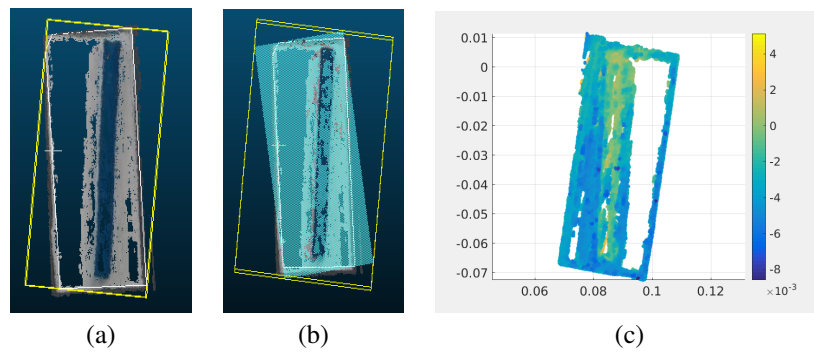
Figure 10-(a) shows an image extracted from

Figure 6: Simulated wound: (a) the selected volume and the polyline around it depicted in yellow, (b) the polyline in yellow and the fitted plane in white, (c) map of distances from each point to the fitted plane.
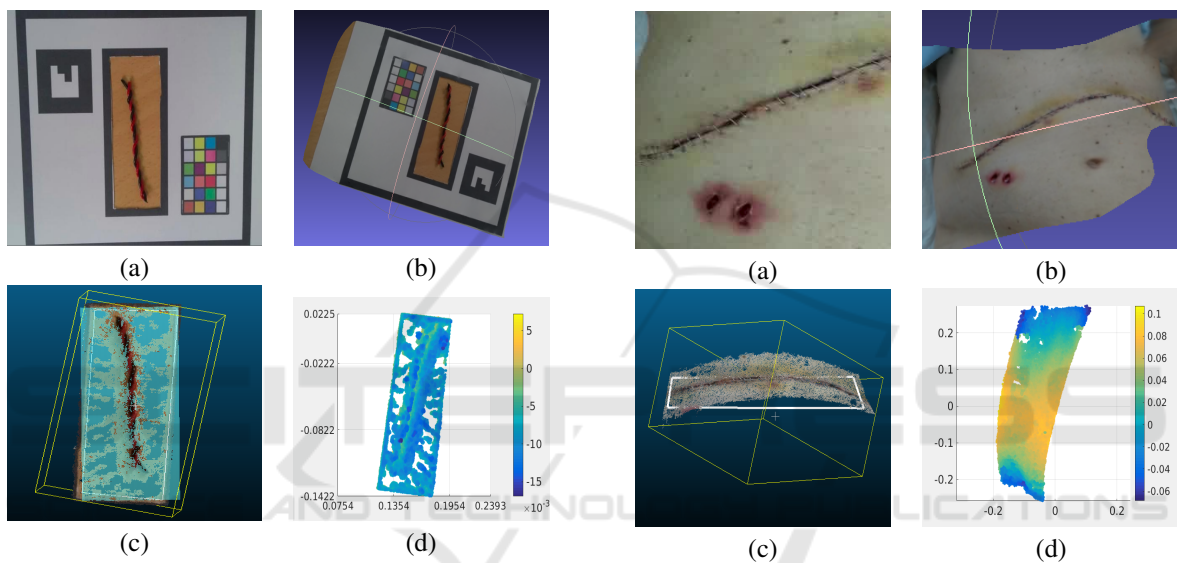

Figure 7: Experiment 2: (a) an image extracted from the video sequence, (b) refined and textured mesh, (c) the wound with the fitted plane depicted in white, (d) Map of distances from each point to the fitted plane.
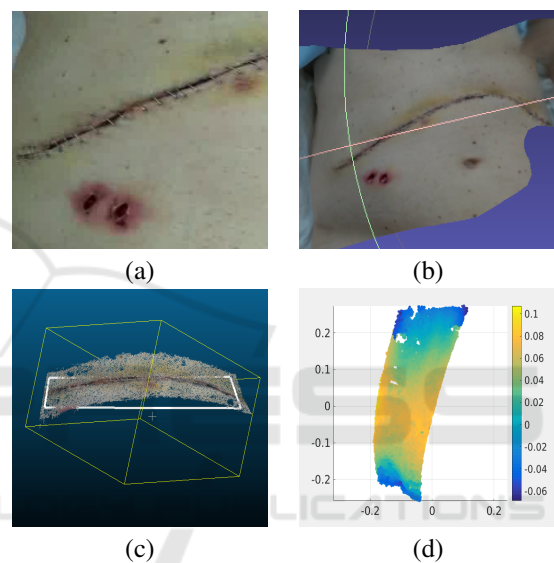

Figure 9: Experiment 4: (a) an image extracted from the video sequence, (b) refined and textured mesh, (c) the wound with the fitted plane, (d) Map of distances from each point to the fitted plane.
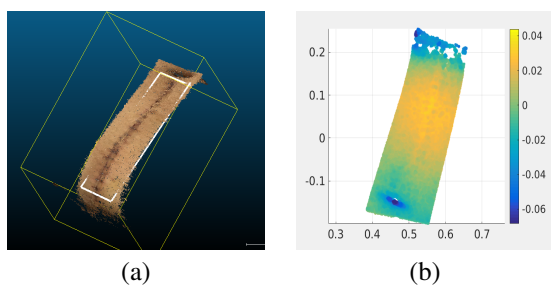

Figure 8: Experiment 3: wound of figure 3: (a) the wound with the polyline and the fitted plane, (b) Map of distances from each point to the fitted plane.

another experiment on a real post-surgical wound grabbed with the template. In this case, the wound presents an evident inflammation of several milimeters. 17 images were extracted from the video to build the 3D model. The scaling factor turned out

to be $0.359m$ in all directions. Figures 10-(b), 10-(c) and 10-(d) show, respectively, the refined textured mesh, the 3D model with the polyline in white fitting the plane, coincident with the template central hole, and the corresponding graphic of distances. The later shows how the points located in the borders of the rectangle present distances between $-5mm$ and $-10mm$, while in the middle, especially in the upper part which coincides with the side of the wound that has the marker at its left and it is clearly below the plane, point distances range between $0mm$ and $5mm$. Although there is a clear gradient of distances between some parts of the center and the sides of the evaluated area, susceptible of being pre-diagnosed as inflamed, the shape of the wound is not clearly identified, being necessary a final and definitive diagnose given by the doctor.
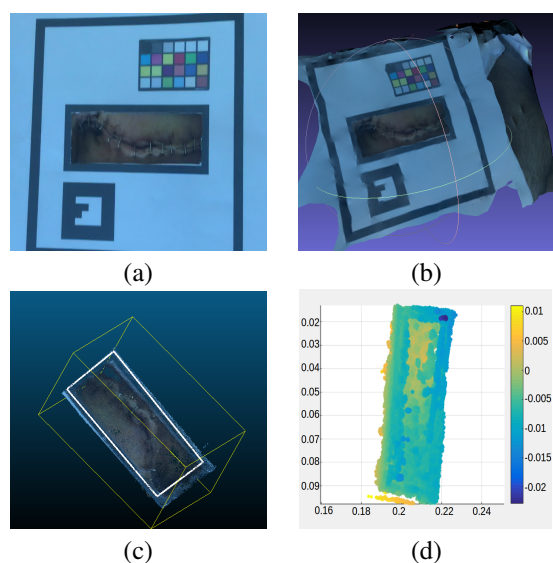
593

(a) (b)

(c) (d)

Figure 10: Experiment 5: (a) an image extracted from the video sequence, (b) refined and textured mesh, (c) the wound with the fitted plane, (d) map of distances from each point to the fitted plane.

Finally, figure 11-(a) shows one frame of a wound which was opened due to an internal infection. Figure 11-(b), figure 11-(c) and figure 11-(d) show, respectively, the refined and colored mesh, the 3D area with the polyline fitting the plane, in white, and the map of distances. The template was put just on the skin, and the plane was fitted around the hole. The distance map evidences a blue zone in the middle corresponding to the opened wound with distances below the plane around $3mm$ ($-3mm$), surrounded by a orange area with distances between $1mm$ and $4mm$ above the plane corresponding to the skin. This gradient of distances marks clearly an anomaly in the area.

The position in which the template is placed on the wound, its adjustment to the abdomen, and the way the plane it fitted in the selected volume affects clearly the obtained results. The procedure needs to be refined, but the initial results are clearly encouraging.

4 CONCLUSIONS

This paper has presented an innovative methodology to estimate a previous diagnose of post-surgical abdominal wounds using visual data. Although experiments with simulated scenes reveal a clear difference between the simulated infected wound and the background, results of experiments with real wounds are still on a preliminary stage, but pointing in a clear good direction. Now the challenge lies, mainly, in
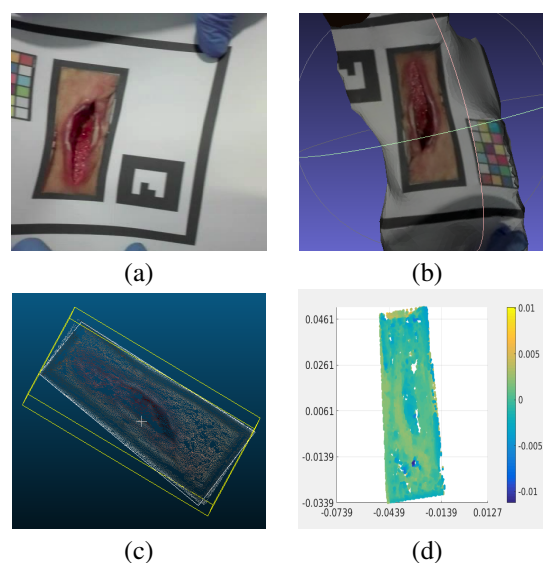

(a) (b)

(c) (d)

Figure 11: Experiment 6: (a) an image from the video sequence, (b) refined and textured mesh, (c) the wound with the fitted plane, (d) map of distances.

two different issues: a) refine the current process to get clearer results, basically testing several possibilities in the positioning of the template and in the generation of the fitted plane, and b) integrating this methodology in a software package, which automatizes all the stages of the process run manually with Cloud Compare to be integrated in a users application.

ACKNOWLEDGEMENTS

REFERENCES

Barnes, C., Shechtman, E., Finkelstein, A., and Goldman, D. (2009). PatchMatch: A Randomized Correspondence Algorithm for Structural Image Editing. *ACM Transactions on Graphics*, 28(3):24:1–24:11.

cDcSeacave (2017). OpenMVS. Open Multi-View Stereo Reconstruction Library. https://github.com/cdcseacave/openMVS.

Girardeau-Montaut, D. (2017). Cloud Compare, 3D Point Cloud and Mesh Processing Software Open Source Project. http://www.danielgm.net/cc/.

Hartley, R. and Zisserman, A. (2003). *Multiple View Geometry in Computer Vision*. Cambridge University Press.

Jancosek, M. and Pajdla, T. (2014). Exploiting Visibility Information in Surface Reconstruction to Preserve

Weakly Supported Surfaces. *International Scholarly Research Notices*, 2014.

Lowe, D. G. (2004). Distinctive Image Features from Scale-Invariant Keypoints. *Int. Journal on Computer Vision*, 60(2):91–110.

Moulon, P., Monasse, P., and Marlet, R. (2013). Global Fusion of Relative Motions for Robust, Accurate and Scalable Structure from Motion. In *Proceedings of the International Conference on Computer Vision*.

Moulon, P., Monasse, P., Marlet, R., and Others (2017). OpenMVG. An Open Multiple View Geometry Library. https://github.com/openMVG/openMVG.

Muja, M. and Lowe, D. (2009). Fast Approximate Nearest Neighbors with Automatic Algorithm Configuration. Source code available at *https://github.com/mariusmuja/flann/*.

Nordheim, L., Haavind, M., and Iversen, M. (2014). Effect of Telemedicine Follow-up Care of Leg and Foot Ulcers: a Systematic Review. *BMC Health Services Research*, 14(565):58–62.

Rublee, E., Rabaud, V., Konolige, K., and Bradski, G. (2011). ORB: An Efficient Alternative to SIFT or SURF. In *Proceedings of the 2011 International Conference on Computer Vision*, pages 2564–2571.

Segura-Sampedro, J., I.Rivero-Belenchón, Pino-Díaz, V., Sánchez, M. R., Pareja-Ciuró, F., Padillo-Ruiz, J., and Rodríguez, R. J. (2017). Feasibility and Safety of Surgical Wound Remote Follow-up by Smart Phone in Appendectomy: A Pilot Study. *Annals of Medicine and Surgery*, 21:58–62.

Topdoctors (2017). Topdoctors. www.topdoctors.es/.

Vu, H., Labatut, P., and Pons, J. (2012). High Accuracy and Visibility-Consistent Dense Multiview Stereo. *IEEE Transactions on Pattern Analysis and Machine Intelligence*, 34(5):889–901.

Waechter, M., Moehrle, N., and Goesele, M. (2014). Let There Be Color! Large-Scale Texturing of 3D Reconstructions. In *Proceedings of the European Conference on Computer Vision*, pages 836–850.